



Combined Experimental and Numerical Simulations of Thermal Barrier Coated Turbine Blades Erosion

*Awatef Hamed, Widen Tabakoff, Rohan Swar, Dongyun Shin, and Nathaniel Woggon
University of Cincinnati, Cincinnati, Ohio*

*Robert Miller
Glenn Research Center, Cleveland, Ohio*

NASA STI Program . . . in Profile

Since its founding, NASA has been dedicated to the advancement of aeronautics and space science. The NASA Scientific and Technical Information (STI) program plays a key part in helping NASA maintain this important role.

The NASA STI Program operates under the auspices of the Agency Chief Information Officer. It collects, organizes, provides for archiving, and disseminates NASA's STI. The NASA STI program provides access to the NASA Aeronautics and Space Database and its public interface, the NASA Technical Reports Server, thus providing one of the largest collections of aeronautical and space science STI in the world. Results are published in both non-NASA channels and by NASA in the NASA STI Report Series, which includes the following report types:

- **TECHNICAL PUBLICATION.** Reports of completed research or a major significant phase of research that present the results of NASA programs and include extensive data or theoretical analysis. Includes compilations of significant scientific and technical data and information deemed to be of continuing reference value. NASA counterpart of peer-reviewed formal professional papers but has less stringent limitations on manuscript length and extent of graphic presentations.
- **TECHNICAL MEMORANDUM.** Scientific and technical findings that are preliminary or of specialized interest, e.g., quick release reports, working papers, and bibliographies that contain minimal annotation. Does not contain extensive analysis.
- **CONTRACTOR REPORT.** Scientific and technical findings by NASA-sponsored contractors and grantees.

- **CONFERENCE PUBLICATION.** Collected papers from scientific and technical conferences, symposia, seminars, or other meetings sponsored or cosponsored by NASA.
- **SPECIAL PUBLICATION.** Scientific, technical, or historical information from NASA programs, projects, and missions, often concerned with subjects having substantial public interest.
- **TECHNICAL TRANSLATION.** English-language translations of foreign scientific and technical material pertinent to NASA's mission.

Specialized services also include creating custom thesauri, building customized databases, organizing and publishing research results.

For more information about the NASA STI program, see the following:

- Access the NASA STI program home page at <http://www.sti.nasa.gov>
- E-mail your question to help@sti.nasa.gov
- Fax your question to the NASA STI Information Desk at 443-757-5803
- Phone the NASA STI Information Desk at 443-757-5802
- Write to:
STI Information Desk
NASA Center for AeroSpace Information
7115 Standard Drive
Hanover, MD 21076-1320

NASA/TM—2013-217857



Combined Experimental and Numerical Simulations of Thermal Barrier Coated Turbine Blades Erosion

*Awatef Hamed, Widen Tabakoff, Rohan Swar, Dongyun Shin, and Nathaniel Woggon
University of Cincinnati, Cincinnati, Ohio*

*Robert Miller
Glenn Research Center, Cleveland, Ohio*

National Aeronautics and
Space Administration

Glenn Research Center
Cleveland, Ohio 44135

April 2013

Acknowledgments

This work was sponsored by the NASA Fundamental Aeronautics Program/Subsonic Totary Wing Project under Cooperative Agreement NNX07AC69A.

Trade names and trademarks are used in this report for identification only. Their usage does not constitute an official endorsement, either expressed or implied, by the National Aeronautics and Space Administration.

This work was sponsored by the Fundamental Aeronautics Program at the NASA Glenn Research Center.

Level of Review: This material has been technically reviewed by technical management.

Available from

NASA Center for Aerospace Information
7115 Standard Drive
Hanover, MD 21076-1320

National Technical Information Service
5301 Shawnee Road
Alexandria, VA 22312

Available electronically at <http://www.sti.nasa.gov>

Combined Experimental and Numerical Simulations of Thermal Barrier Coated Turbine Blades Erosion

Awatef Hamed, Widen Tabakoff, Rohan Swar, Dongyun Shin, and Nathaniel Woggon
University of Cincinnati
Cincinnati, Ohio 45220

Robert Miller
National Aeronautics and Space Administration
Glenn Research Center
Cleveland, Ohio 44135

Abstract

A combined experimental and computational study was conducted to investigate the erosion of thermal barrier coated (TBC) blade surfaces by alumina particles ingestion in a single stage turbine. In the experimental investigation, tests of particle surface interactions were performed in specially designed tunnels to determine the erosion rates and particle restitution characteristics under different impact conditions. The experimental results show that the erosion rates increase with increased impingement angle, impact velocity and temperature. In the computational simulations, an Euler-Lagrangian two stage approach is used in obtaining numerical solutions to the three-dimensional compressible Reynolds Averaged Navier-Stokes equations and the particles equations of motion in each blade passage reference frame. User defined functions (UDF) were developed to represent experimentally-based correlations for particle surface interaction models which were employed in the three-dimensional particle trajectory simulations to determine the particle rebound characteristics after each surface impact. The experimentally based erosion UDF model was used to predict the TBC erosion rates on the turbine blade surfaces based on the computed statistical data of the particles impact locations, velocities and angles relative to the blade surface. Computational results are presented for the predicted TBC blade erosion in a single stage commercial APU turbine, for a NASA designed automotive turbine, and for the NASA turbine scaled for modern rotorcraft operating conditions. The erosion patterns in the turbines are discussed for uniform particle ingestion and for particle ingestion concentrated in the inner and outer 5 percent of the stator blade span representing the flow cooling the combustor liner.

Introduction

Turbomachinery erosion presents a challenging problem when gas turbine engines operate in dusty environments (Refs. 1 to 3). Some of the mechanisms that cause particle ingestion are (a) the vortex from engine inlet-to-ground during high power setting with the aircraft standing or moving on the runway; (b) storms transporting sand to several thousand feet altitude; (c) thrust reverser afflux at low airplane speed blowing sand, ice and other particles into the engine inlets. Erosive solid particles may also be produced during the combustion process, from the burning of different types of heavy oils or synthetic fuels. Helicopter engines are especially susceptible to large amounts of dust and sand ingestion during hover, takeoff and landing.

It is very difficult to remove all solid particles from the gas stream without taxing the performance of gas turbine engines (Refs. 4 and 5). Even small particles of 1 to 30 μm size have been known to be very damaging to the exposed components of coal burning turbines (Ref. 6). In turbomachinery, particle impacts are known to increase tip clearances and blade surface roughness and produce changes in the blade leading and trailing edges (Ref. 7). Because TBC erosion is detrimental to the thermal protection of turbine blades, it has been identified as a life limiting factor for gas turbines (Refs. 8 to 10). With the

increasing use of thermal barrier technology to protect highly loaded and rotating turbine components (Ref. 11), further studies are needed to support thermal protection for life extension.

Different process combinations such as cutting, fatigue, brittle fracture and melting mechanisms have been proposed to govern material removal by erosion. According to experimental studies of blade alloys and coating materials, their erosion rates are influenced by particle impact velocities and impingement angles and by the operating temperatures (Ref. 3). Experimental characterization of material erosion resistance requires special facilities that control particle-laden flow around the sample to achieve the desired impact conditions over the tested samples (Ref. 12). Prior TBC erosion test results have demonstrated that electron beam-physical vapor deposited (EB-PVD) TBC erosion rates are an order of magnitude less than plasma sprayed (PS) TBC and that both increase linearly with particles impact velocity (Refs. 13 and 14). Experimental studies of particle surface impacts are also necessary to provide particle rebound characteristics over the range of impinging conditions encountered in turbomachines (Refs. 3 and 7).

Blade erosion in turbomachines is affected by rotational speed and flow conditions, blade geometry and blade row location, blade material and particle characteristics (Refs. 3 and 7). Under two-phase flow conditions, the gas and particles experience different degrees of turning through the blade passages. Deviation from the gas flow path increases with particle inertia causing repeated impacts with the various surfaces. Surface impacts alter the direction and velocity of the particles as well as their distribution through subsequent stages. Experimental studies that simulate erosive particle impact conditions in the engine environment are essential to blade and coating material development. The associated blade surfaces erosion requires knowledge of the particle three-dimensional trajectories and their impact statistics on the various engine surfaces in addition to surface material erosion behavior under the impact conditions.

Trajectory simulations are based on the numerical integration of the particles' equations of motion through the successive turbomachinery stationary and rotating blade rows. The simulations require the three-dimensional flow field and blade passage geometries as inputs and a model for particle restitution conditions following each surface impact. The basis for particle trajectory simulations in turbomachines continues to be Eulerian-Lagrangian with one way coupling between the particles and flow (Refs. 15 and 16). Currently three-dimensional flow field solutions of the Reynolds Averaged Navier-Stokes equations for turbulent flow through the blade passages (Ref. 16) are used in turbomachinery trajectory simulations.

Hamed and Tabakoff (Ref. 17) developed a methodology to predict turbomachinery blade surface erosion using blade surface statistical impact data computed from particle trajectory simulations and correlations based on blade material erosion test results. It was used in the prediction of blade erosion in both axial and radial compressors and turbines (Ref. 3) and erosion of turbine blade coating developed for automotive and ground based gas turbine applications.

In the current work, a combined experimental and numerical investigation was conducted to study the deterioration of thermal barrier coating on turbine blades by erosive particles. Experimental measurements were obtained for EB-PVD 7YSZ/PtAl coated Inconel 718 coupons in the high temperature erosion tunnel under different impact conditions by alumina particles. Measurements were also obtained for particle restitution characteristics at different impact angles relative to the coated sample using Particle Image Displacement Velocimetry (PIDV). The experimental measurements of surface erosion and particle restitution were used to develop empirical erosion and restitution models. The numerical simulations for the three-dimensional flow field and particle trajectories were combined with experimentally based surface interaction models to predict TBC erosion over the stator and rotor blade surfaces in a single stage commercial gas turbine and in a NASA automotive turbine design (Ref. 18) and scaled for modern rotorcraft operating conditions (Ref. 19).

Experimental Work

Erosion tests were carried out for 25.4 by 25.4 by 1.5875 mm (1 by 1 by 1/16 in.) Inconel 718 coupons coated with EB-PVD 7YSZ over a range of impact conditions by different size alumina particles. The coupons were mounted on a sample holder and placed at the designated angles in the high temperature

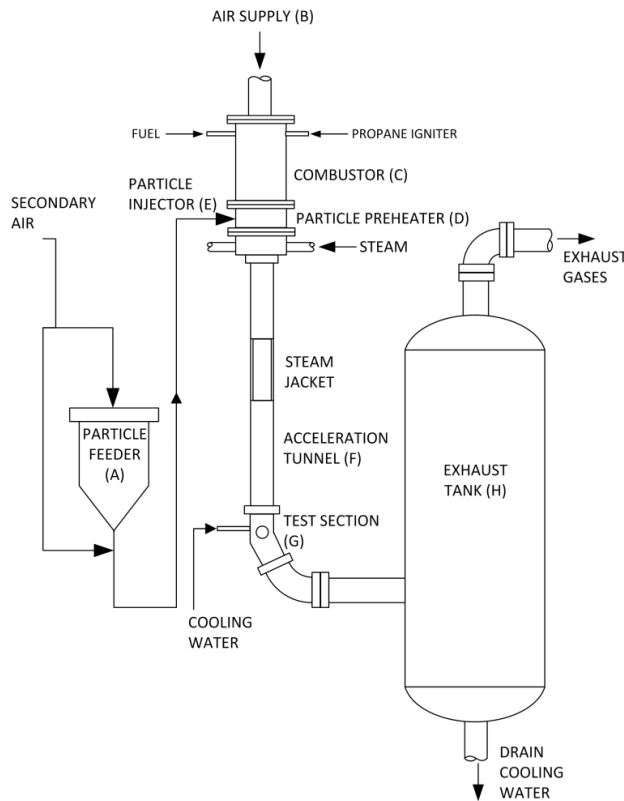


Figure 1.—Schematic of erosion test facility.

erosion wind tunnel shown schematically in Figure 1 and subjected to erosion by a calibrated mass of particles. The holder protected all but one target coupon surface that was exposed to particle impacts. The samples were weighed before and after the erosion tests to determine the weight loss due to erosion by the impacting particles.

The University of Cincinnati (UC) erosion wind tunnel (Ref. 12) shown schematically in Figure 1 consists of the following components: particle feeder (A), main air supply pipe (B), combustor (C), particle pre-heater (D), particle injector (E), acceleration tunnel (F), test section (G) and exhaust tank (H). Abrasive particles of a given constituency and measured weight are placed into the particle feeder (A). The particles are fed into a secondary air source and blown into the particle preheater (D) and then to the injector (E), where they mix with the primary air supply (B), which is heated by the combustor (C). The particles are then accelerated via high velocity air in a constant-area steam-cooled duct (F) and impact the specimen in the test section (G). The particulate flow is then mixed with coolant and directed to the exhaust tank. As can be seen from Figure 1, the tunnel geometry is uninterrupted from the acceleration tunnel throughout the test section in order to preserve the aerodynamics of the flow passing over the samples. Particles' impact velocities are calibrated with the tunnel air flow, while the particle impingement angle is controlled through the sample orientation. A measured mass of particles is fed into the flow after the test sample reaches equilibrium temperature.

The erosion rate, ϵ in mg/g is defined as the ratio of the measured coated sample erosion mass loss, ΔW , to the mass of erosive particles impacting surface, Q_p , which is determined from the tunnel calibration according to the sample size and impingement angle (Ref. 20).

$$e = \frac{DW}{Q_p} \quad (1)$$

Particle restitution characteristics after impacting the coated coupons were measured in a second tunnel equipped with optical window in the test section for recording particle trajectories using high speed photographic methods at room temperature. A Phantom high speed digital camera (model V 9.1) with a Nikon lens was used to photograph the particle trajectories. The camera had a maximum frame speed of 50,000 fps, but a frame rate of 27,000 fps (37 μ s interval) and 256 \times 256 resolution were appropriate for the light intensity obtained from a 250 mW Spectra-Physics laser source (454 to 676 nm wavelength). Referring to Figure 2, the laser sheet was 1.65 mm thick and 50 mm in height at the frame of interest and the exposure time could be set as low as 3 μ s. The camera was connected to a computer and its graphical user interface (GUI) software was used to set the frame speed and resolution, after it was focused on a reference point in the laser sheet before recording the images.

The magnitude and direction of the particle impact and rebound velocities were measured in the plane of the laser sheet. The x and y co-ordinates of a particle in each frame were determined using Phantom Cine Viewer image processing software. By comparing successive images, the trajectory of the particle was calculated using Particle Image Displacement Velocimetry (PIDV) technique (Refs. 21 to 23). The image of a 25.4 mm mark was used as a reference length to provide the actual distance the particle traveled between successive frames as shown in Figure 3. The particle velocity, V , was calculated based on the time between two successive frames:

$$V = \frac{dS}{dt} = \frac{FRd}{r} \quad (2)$$

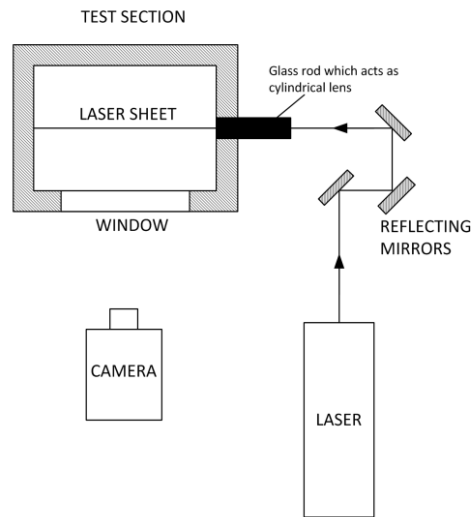


Figure 2.—Test section, laser sheet and camera.

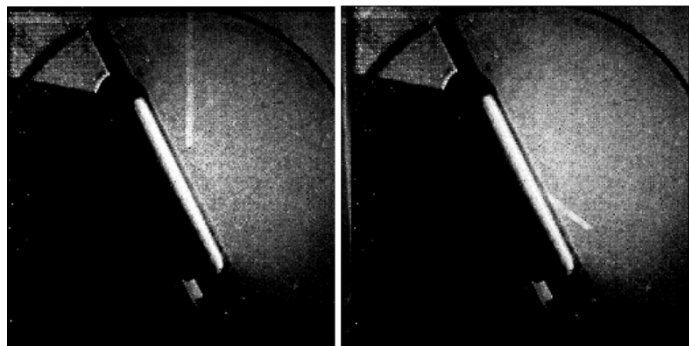


Figure 3.—High speed photography images.

Where:

- δt time between successive frames, sec
- F number of frames per second
- V particle velocity
- δS actual distance traveled by particle between two consecutive frames
- R actual length of the reference mark in the test section
- d distance traveled by particle as obtained from the pixel count
- r length of the reference mark as obtained from the pixel count

The velocity and directional restitution coefficients were determined from three successive frames of interest in order to exclude the post impact influence of the tunnel flow on the rebounding particle trajectory. Error estimations of the results obtained from high speed photography were carried out using the t-distribution method (Ref. 23) with 95 percent confidence interval.

Computational Work

Numerical simulations were conducted using ANSYS CFX 12 (Ref. 24) to calculate the three-dimensional flow field and the associated 26 μm particle trajectories in a single stage gas-turbine. The Eulerian-Lagrangian two stages, one-way particle interaction model approach was used because of the typically low particle concentration in gas turbines.

Pointwise V16 (Ref. 25) code was used to generate the structured computational grids in the stator and rotor blade passages of the single stage turbines. Its elliptic solver was used to improve the grid quality especially in the high turning rotor blade passage. Figure 4 shows the three-dimensional H-O computational grids used in the NASA designed turbine flow field and particle dynamics simulations. Grid size was based on our prior experience in large commercial engines (Ref. 16). The grids were clustered near the blade passage surfaces to achieve the $y^+ < 3$ at the first grid point next to the surface.

The three-dimensional flow field solutions were obtained for the compressible Reynolds-Averaged Navier-Stokes equations in conservation form and the $k-\omega$ based Shear-Stress-Transport (SST) model. Advection fluxes were evaluated using the high-resolution scheme in ANSYS CFX 12 (Ref. 24) which is second-order accurate with convergence criteria of 10 to 5 rms residual. Because of the very high particle velocities in the turbine particularly after rebounding from rotor blade surface impacts, the turbulence stochastic effects are negligible and the aerodynamic forces on the particles are dominated by drag due to particle slip velocities relative to the gas velocities.

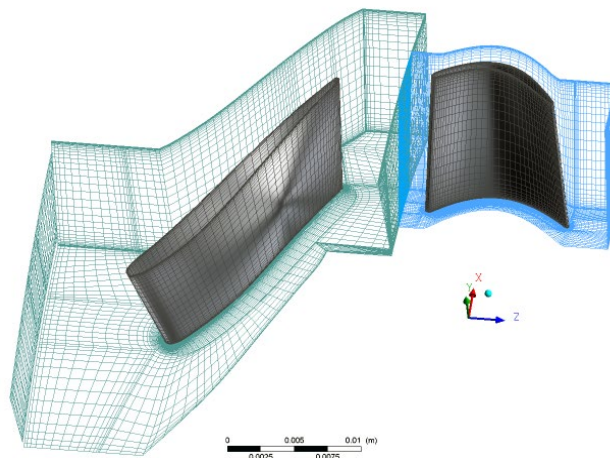


Figure 4.—Sample computational grids of the NASA designed turbine.

The total pressure, total temperature inlet and flow direction were specified at the inlet boundary and uniform averaged static pressure was specified at the outlet boundary with the periodic interface boundary conditions invoked in the stator and rotor blade passages. A mixing plane model was used at the stator-rotor interface. The simulations were conducted for particles entering the turbine in the same direction as the inlet gas flow but with 50 percent the value of the inlet gas velocities.

The nominally 26 μm erosive alumina particles were assumed to be ingested at the same temperature as the gas inflow. Convective heat transfer coefficient based on ANSYS CFX 12 (Ref. 24) correlation represented the interphase energy exchange. Particle trajectories were computed using forward integration and taking into consideration the momentum and heat exchange with the flow field based on the three-dimensional flow solutions. The particle tracking integration time step was chosen locally such that the particles were advanced 100 time steps within each grid spacing used to obtain the three-dimensional turbine flow solutions (Ref. 24).

Particle surface interaction modeling was based on experimental data obtained for TBC coated samples over a range of impact conditions by the alumina particles. The restitution and erosion prediction empirical models were implemented in ANSYS CFX 12 (Ref. 24) as user-defined functions.

Results and Discussions

Experimental Results

Figure 5 presents sample results for the experimentally measured erosion rates variation with particle impingement angles for 10 mil EB-PVD 7YSZ coated Inconel 718 samples and for samples of the Inconel 718 substrate at 1093 $^{\circ}\text{C}$ (2000 $^{\circ}\text{F}$) temperature and 366 m/s (1200 ft/s) impact velocity. The maximum erosion rate for the EB-PVD TBC coating occurred at 90 $^{\circ}$ impingement angle while that for INCO substrate occurred between 20 $^{\circ}$ to 30 $^{\circ}$ which are typical brittle and ductile materials erosion behavior, respectively. One can see from Figure 6(a) that the nominally 26 μm , mass mean erosive alumina particles have angular shapes with sharp corners. The particles size distribution is shown in Figure 6(b).

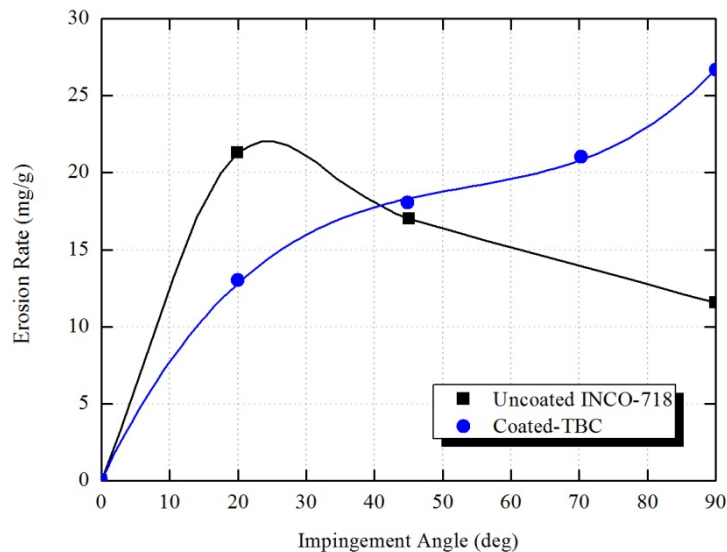
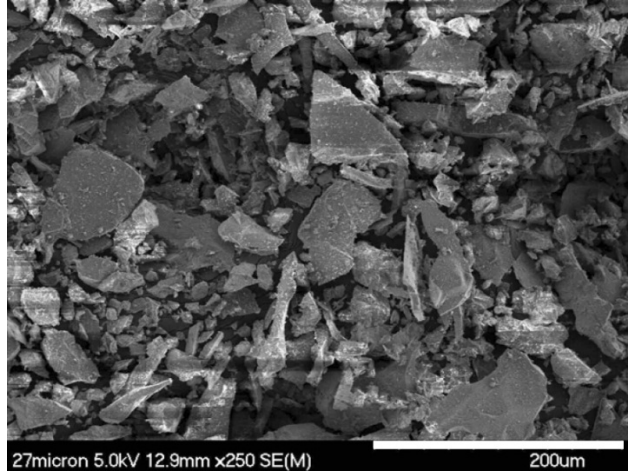
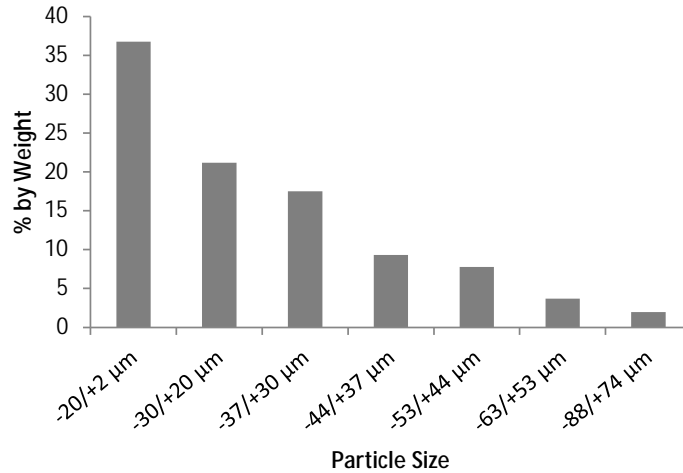


Figure 5.—Measured erosion rates due to 26 μm alumina particle impacts on TBC coated and uncoated samples ($T = 1093$ $^{\circ}\text{C}$ (2000 $^{\circ}\text{F}$), $V = 365.8$ m/s (1200 ft/s)).



(a) Scanning electron microscope image of sample particles.



(b) Particle size distribution by weight.

Figure 6.—Nominally 26 μm alumina particles.

Figures 7 and 8 present experimental results for EB-PVD TBC erosion rates variation with impingement angles at 982 °C (1800 °F) and 871 °C (1600 °F), respectively. According to these results the erosion rates increase with temperatures and with particle impact velocities at all impingement angles. This is consistent with the TBC erosion test results presented at 90° impact angle in prior investigations by Tabakoff (Ref. 13) and Nicholls et al. (Ref. 14). The following experimentally based TBC erosion rate correlations were implemented in the UDF and used in ANSYS CFX 12 (Ref. 24) to compute the TBC erosion rates on the blade surfaces based on the local gas temperature T , particle impact velocity V_1 and impingement angle b_1 , relative to the coated blade surface.

$$e = \left(1.293b_1 - 1.301b_1^2 + 0.473b_1^3\right)(3.28V_1)^n \quad (3)$$

Where:

$$n = 0.0584 + 0.000476T$$

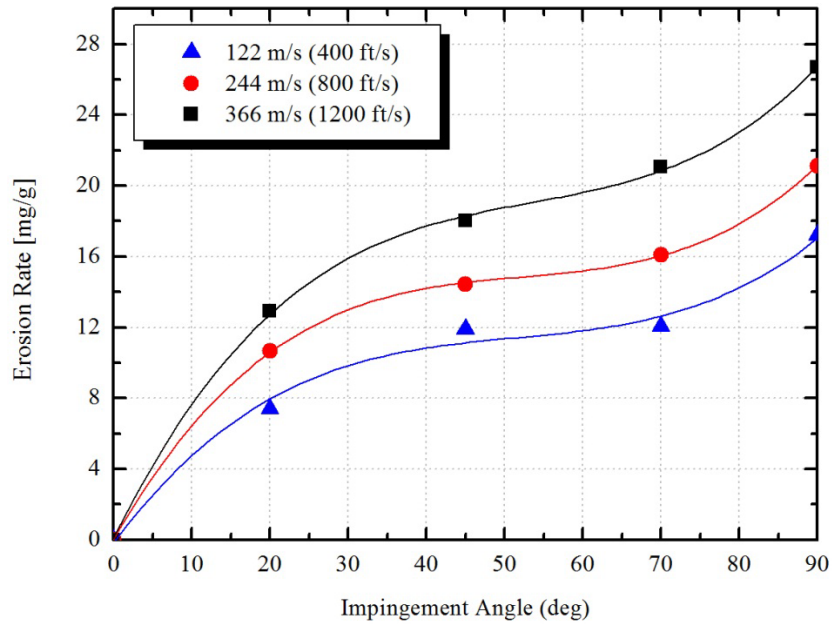


Figure 7.—TBC erosion rates by 26 μm alumina particles at 982 °C (1800 °F).

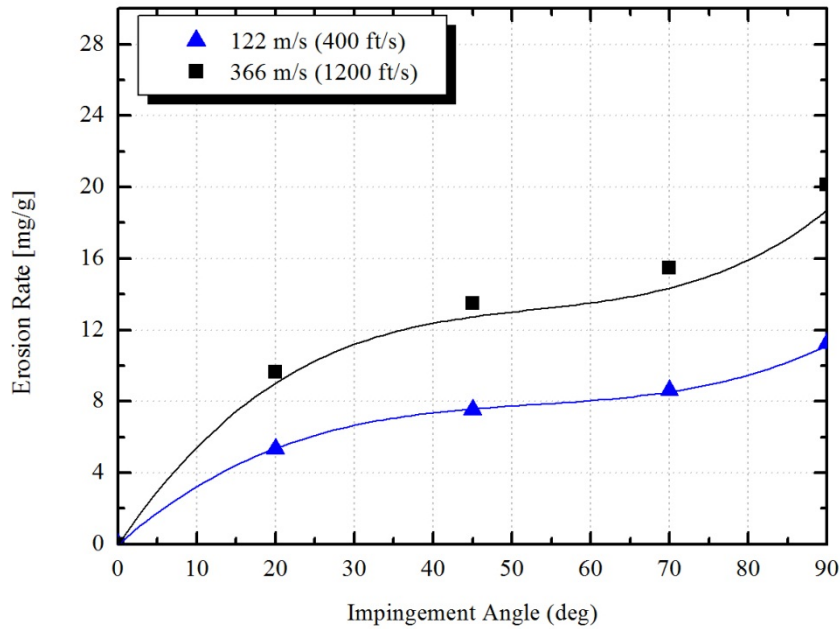


Figure 8.—TBC erosion rates by 26 μm alumina particles at 871 °C (1600 °F).

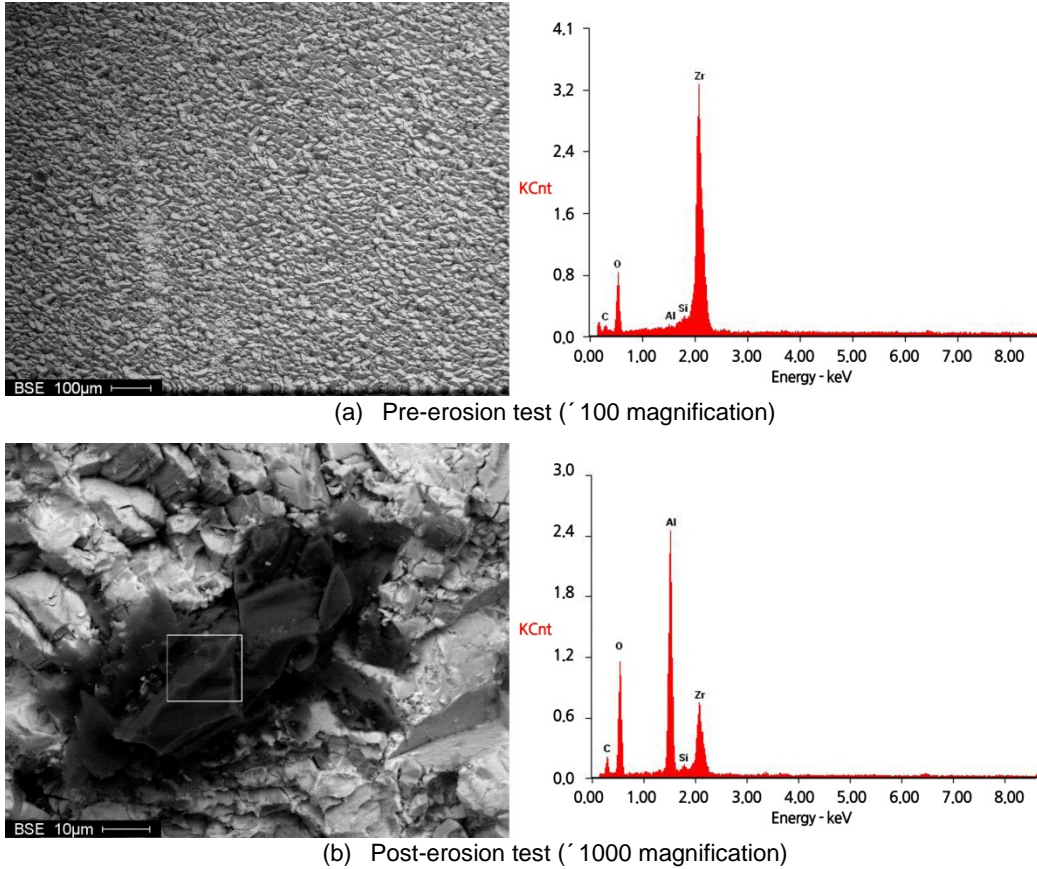


Figure 9.—Sample TBC surface scans with electron microscope.

Several post erosion tested samples were examined using Scanning Electron Microscope to investigate post erosion particle deposition. Sample results are presented in Figure 9 for pre and post erosion test samples. Particle deposition was rarely observed on the post erosion test samples, as shown in the post erosion ~ 1000 magnification image.

The experimental results were used to derive the particle velocity and angle restitution coefficients e_v and e_b relative to the impacted turbine coated surfaces as a function of the particles impingement angle b_1 .

$$e_v = \frac{v_2}{v_1} = 0.5 + 1.9369b_1 - 4.0075b_1^2 + 3.1881b_1^3 - 0.8218b_1^4 \quad (4)$$

$$e_b = \frac{b_2}{b_1} = 0.9832 + 0.474b_1 - 3.5837b_1^2 + 3.4188b_1^3 - 0.9569b_1^4 \quad (5)$$

However, ANSYS CFX 12 (Ref. 24) requires user defined functions in the form of restitution coefficients that are normal and tangential to the impacted surface. The experimental correlations of Equations (5) and (6) were therefore used to compute the normal and tangential restitution coefficients e_n and e_t that are presented in Figure 10 using the following equations:

$$e_n = e_v \frac{\sin(b_1 e_b)}{\sin(b_1)} \quad (6)$$

$$e_t = e_v \frac{\cos(b_1 e_b)}{\cos(b_1)} \quad (7)$$

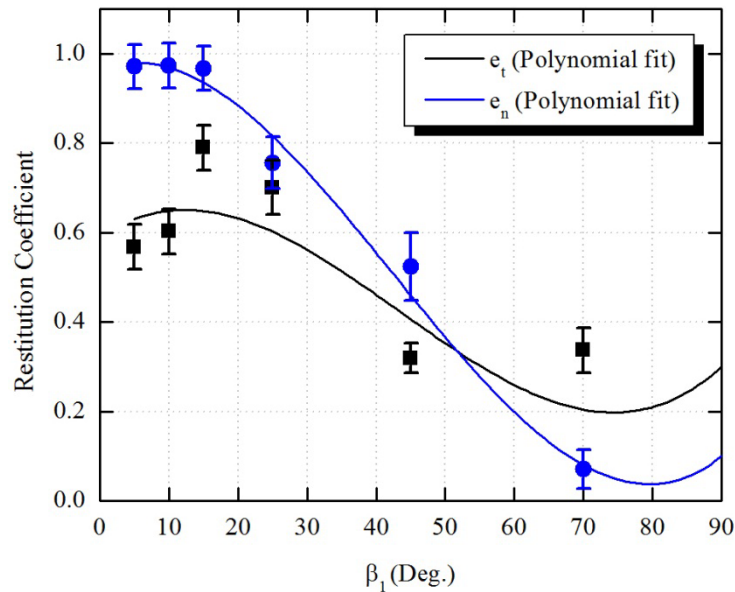


Figure 10.—Particle tangential and normal restitution coefficients variation with impact angles.

Numerical Predictions of Turbine Blades TBC Erosion Based on Computed Three-Dimensional Flow Fields and Suspended Particle Trajectories Incorporating Experimentally Based Particle Surface Interaction Model

Three sets of numerical predictions of three-dimensional turbine flow fields, particle trajectories turbine blades TBC erosion are presented for (1) commercial APU turbine (2) NASA designed automotive turbine (Ref. 18) (3) a scaled version of NASA designed turbine for modern rotorcraft operating conditions (Ref. 19).

The particle material property used was 99 percent aluminum oxide (alumina). A density of 3.96 g/cc and a molecular weight of 101.961 g/mol described the particles' mass. All particles were 26 μm in diameter with an initial velocity in the axial direction of 64 percent of the gas flow velocity at the inlet plane.

Commercial APU Turbine

Figure 11 presents carpet plots of the computed absolute Mach number at mid-span through the stator and the relative Mach number through the rotor, while Figure 12 presents the corresponding static pressure. The blade wakes are visible in Figure 11 and also a strong expansion wave at the rotor pressure surface trailing edge that extends across the blade passage towards the opposite blade suction surface is visible in both Figures 11 and 12. The two figures also indicate a second shock emanates off the rotor trailing edge suction surface and propagates downstream.

Figure 13 shows 25 sample trajectories with color contouring of their velocity magnitude for 26 μm alumina particles seeded uniformly across the turbine inlet. The figure indicates that after the particles enter the stator blade row flow field they continue along their axial path until they impact the stator blade surface. Mainly at the pressure surface and the leading edge of the suction surface. The particles then enter the rotor blade passage and impact the suction surface of the rotor blade because of their lower absolute velocities compared to the gas flow as they leave the stator and enter the rotor as demonstrated by their absolute and relative velocities shown schematically in Figure 14. The particles rebound with high circumferential velocities after their rotor blade suction surface impacts that cause them to travel radially outward to the shroud. Many particles are seen to reenter the stator blade passage and impact

the aft portion of the stator blades suction surface with the high velocities they acquired from the rotor blade surface impacts. Some particles reenter the stator blade passage only momentarily then are dragged by the flow back into the rotor blade passage. Eventually the majority of these particles continue to travel down the rotor blade passage impacting the pressure surface of the turbine rotor at a significantly lower velocity.

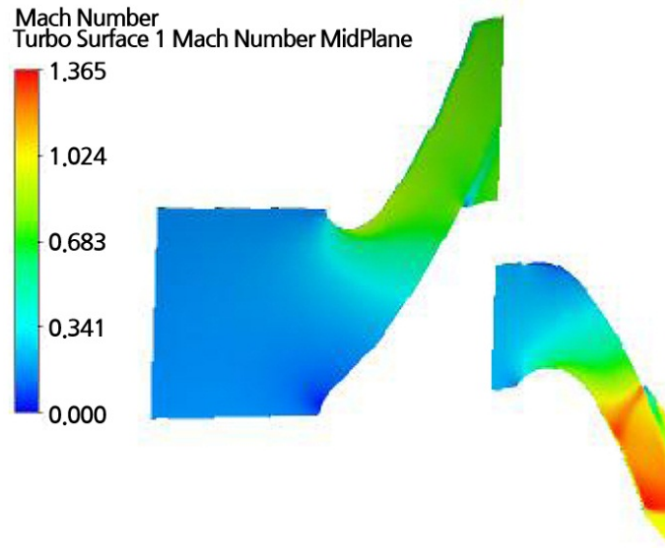


Figure 11.—Mach number contours at the 50 percent blade span (Commercial APU Turbine).

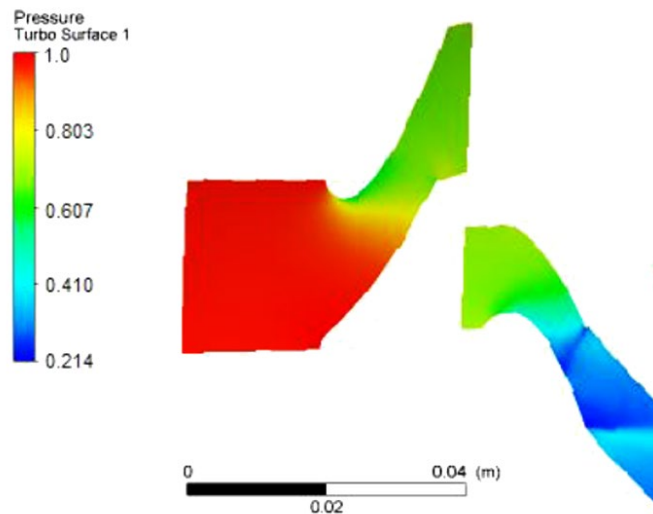


Figure 12.—Computed normalized pressure near mid-span (Commercial APU Turbine).

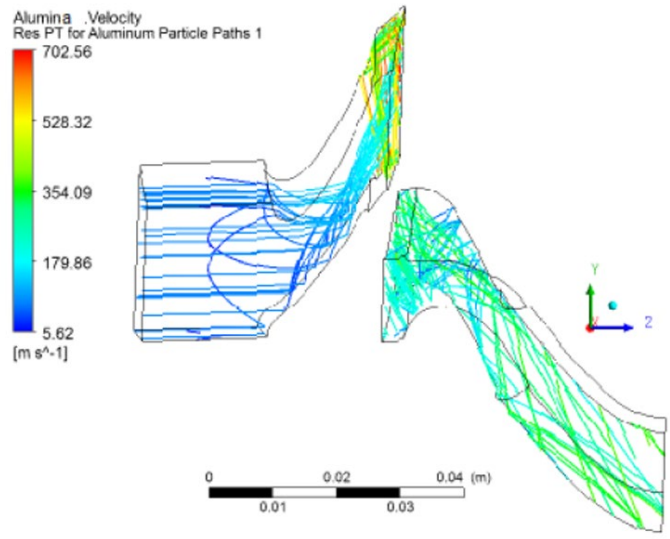


Figure 13.—Sample three-dimensional particle trajectories in the commercial APU turbine.

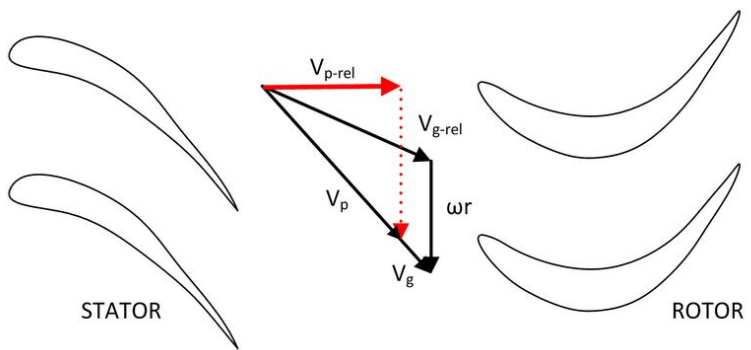


Figure 14.—Schematic showing effect of particle slip velocity at the stator exit on entrance condition in the rotor reference frame.

Figure 15 presents the predicted thermal barrier coating erosion rates on the stator and rotor blades of the commercial APU turbine. The figures indicate relatively low uniform thermal barrier coating erosion rate on the aft half of the stator blade pressure surface and high erosion rates on the stator blade suction surface at the corner of the tip and trailing edge. This high erosion rate on the stator suction surface is caused by the high velocity particles that reenter the stator blade row after impacting the rotor suction surface because they lag the gas flow as they leave the stator blade row (Fig. 14). These same particles produce the highest erosion rate of the rotor blade suction surface at the shroud and leading edge corner. The particles are concentrated near the shroud by the centrifugal forces after they impact the rotor suction surface and gain the highest relative velocity. Several of the particles have second impacts as they reenter the rotor blade passage near the tip after they rebound from the stator suction surface impacts.

Figure 16 presents the computed results for particle trajectories when the particles are seeded only within 5 percent of the stator span at the hub and shroud. This seeding represents the suspended particle in the cooling secondary flow. Trajectory trends are similar to the previous case. The only obvious difference is the lack of particle impacts in the middle of the stator span due to the seeding locations. However, the particles seeded near the hub are still immediately thrown to the shroud when they impact the rotor blade suction surface. As the particles travel through the rotor they become concentrated at the shroud just as in the previous case.

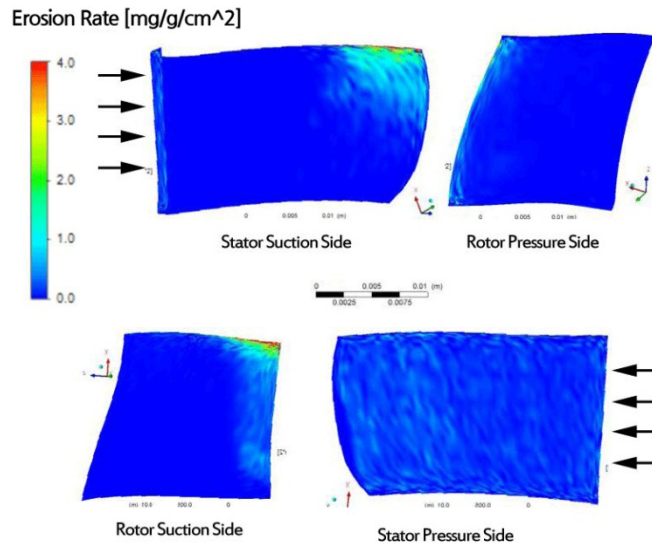


Figure 15.—TBC erosion rates on blade surfaces in the commercial APU turbine for particle ingested at 50 percent the gas velocity with uniform radial loading.

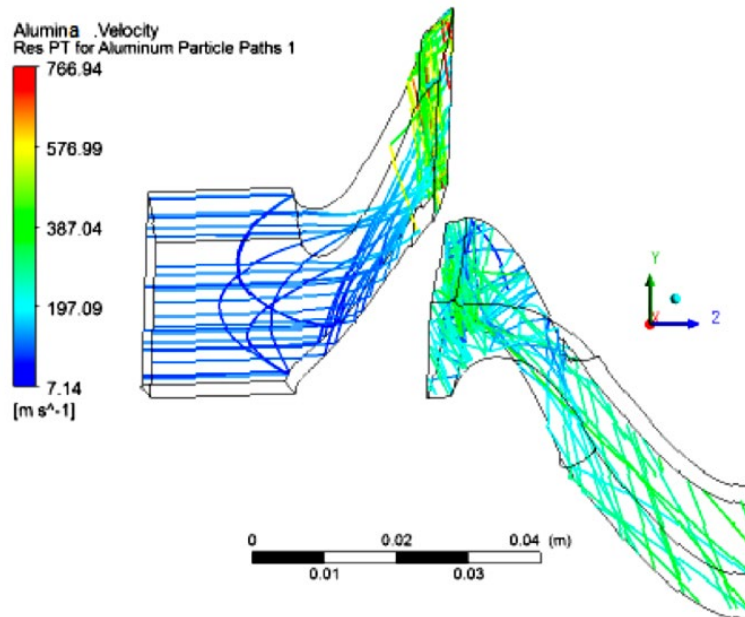


Figure 16.—Computed three-dimensional particle trajectories for particle seeding within 5 percent of the rotor span and using the experimentally based UDF restitution model.

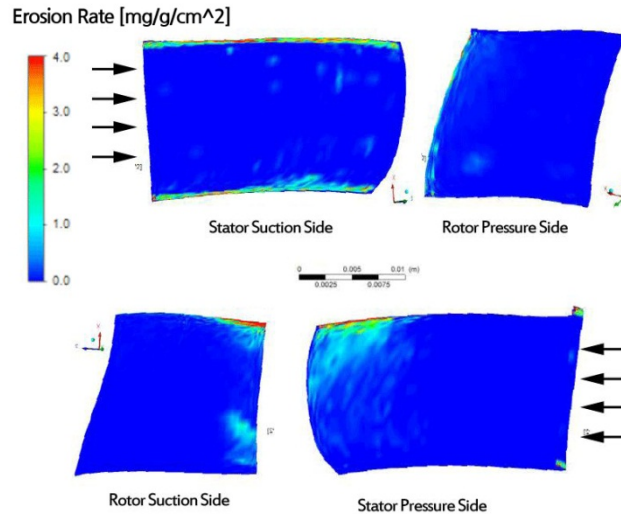


Figure 17.—TBC erosion rates on blade surfaces in the commercial turbine for particle seeding within 5 percent of the rotor span at 50 percent of the gas velocity.

TABLE 1.—COMPUTED OVERALL BLADES AND MAXIMUM LOCAL TBC EROSION RATES ON THE COMMERCIAL APU TURBINE

Turbine	Particle radial loading% span	Maximum local erosion rate, mg/g/cm ²	Overall blade erosion rate, mg/g	
			Stator	Rotor
APU commercial turbine	5%	72.94 (Rotor suction side)	0.78	0.93
	100%	31.16 (Stator suction side)	0.83	0.87

Figure 17 shows the corresponding thermal barrier coating erosion rates on the stator blade surfaces when the particles are seeded only within 5 percent of the stator span at the hub and shroud. Erosion on the stator pressure surface is seen to occur almost exclusively along these thin bands. Again the highest erosion rate is at the shroud and trailing edge corner of the stator blade suction surface that is caused by the particles reentering the stator near the tip with higher velocities after impacting the rotor suction surface. The dominance of the centrifugal forces on the particles after their impacts with the rotor is evident even in the trajectories of the particles that were originally concentrated at the hub.

A list of the predicted local maximum as well as the overall TBC erosion rates in the APU commercial turbine stator and rotor blades for both uniform and non-uniform particle injection is presented in Table 1.

In summary, the highest thermal barrier coating erosion rate in the APU turbine is always predicted on the rotor blade surface. This occurs mostly towards the shroud near the leading edge on the rotor suction surface. On the other hand, the pressure surface of the rotor always suffers the lowest thermal barrier coating erosion rate. Numerical simulations of particle trajectories were also conducted with a uniform restitution model based on the average value of the experimental measurements (Ref. 26).

NASA Designed Original and Scaled Turbine for Modern Rotorcraft Operating Conditions

Numerical predictions of the three-dimensional flow field, particle trajectories and TBC blade coating erosion were conducted for a NASA designed automotive turbine whose geometry and operational characteristics are in the public domain as listed in Table 2 (Ref. 18). The original turbine operational conditions were scaled to meet the requirements of a modern rotorcraft engine comparable to Bell Ranger 206 (Ref. 19). As shown in Table 3, the mass flow rate and rotating speed of the scaled turbine were based on the use of the following turbomachinery scaling laws:

$$\frac{r_h}{\sqrt{p_{01} D^2}} \sqrt{\frac{RT_{01}}{p_{01} D^2}} = \text{constant}; \frac{ND}{\sqrt{(RT_{01})}} = \text{constant} \quad (8)$$

TABLE 2.—NASA DESIGNED
AUTOMOTIVE TURBINE
(TMX-71717) GEOMETRY

Blade row	Stator	Rotor
Pitch, cm	2.096	0.5621
Mean chord, cm	2.311	1.043
Height, cm	1.118	1.105
L.E. radius, cm	0.0635	0.0331
T.E. radius, cm	0.0191	0.0191
Number of blades	15	56

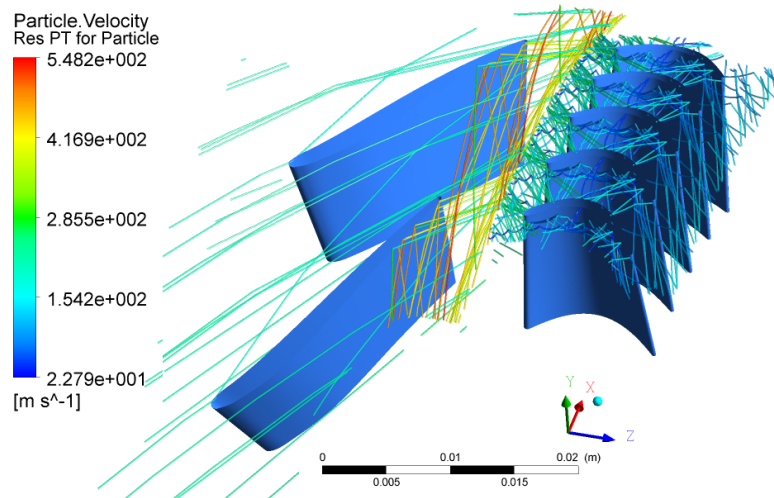
TABLE 3.—OPERATING CONDITIONS FOR ORIGINAL NASA DESIGNED TURBINE AND SCALED TURBINES

Parameters	NASA 1979 design Automotive turbine TMX-71717	Scaled NASA turbine
Inlet total temperature	1325 (°K)	1900 (°K)
Inlet total pressure	3.92 (atm)	17 (atm)
Mass flow rate	0.598 (kg/s)	2.166 (kg/s)
Rotor speed	6126.9 (rad/s)	7335.9 (rad/s)
Shaft power	22.615 [kW]	134.747 [kW]
Reaction	0.8013	0.8335
Total-to-total Polytrophic efficiency, percent	78.5385	87.6644

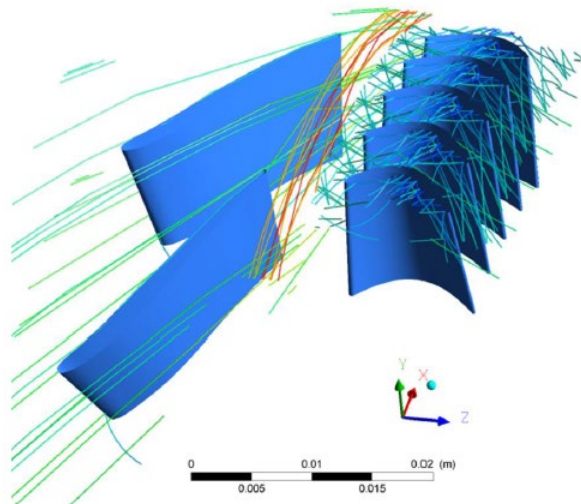
Referring to Table 3, the scaled turbine produces about 6 times the shaft power at 3.6 times the mass flow rate because of the 4.33 times higher intake total pressure. The other hand, the inlet flow stagnation temperature for the scaled turbine is only 1.433 times the NASA original turbine Figures 18 and 19 present computed Mach number and static pressure carpet plots at 50 percent blade span for the NASA 1975 designed and scaled turbines in the reference frame of each blade row. The contours indicate slightly higher Mach numbers in the scaled turbine compared to the original turbine.

Figures 20 presents sample trajectories with color contouring of their velocity magnitude for 26 μm alumina particles in the NASA designed turbine (Fig. 20(a)) and scaled NASA turbine (Fig. 20(b)) corresponding to particle seeding within 5 percent of the span near the hub and shroud. Most particles are seen to go through the stator blade passages with negligible interactions with the blade surfaces. However as they enter the rotor blade passages, they impact the rotor blades suction surface towards the leading edge in the NASA designed original turbine. The particles rebound with high circumferential velocities after their rotor blade suction surface impacts, which immediately drive them radially outward and back into the stator blade passages. In contrast, particles encounter multiple impact within the rotor blades row in the scaled NASA turbine but do not rebound back into the stator blade passages.

Figures 21 and 22 present the predicted thermal barrier coating erosion rates for the NASA designed original turbine stator and rotor blade surfaces corresponding to uniform particle seeding (Fig. 21) and particle seeding within 5 percent of the span near the hub and shroud to represent suspended particles in the cooling secondary flow (Fig. 22). In both cases, high erosion rates are seen on rotor blades suction surface at the shroud close to the leading edge and on the stator blades suction surface at the casing near trailing edge. The latter are associated with the repeated impacts by the particles that get trapped and bounce back and forth between the rotor and stator blade rows. Since the particles acquire the highest absolute velocities when they rebound from the rotor suction surface impacts, they produce the highest erosion rates by their subsequent impacts the stator blade suction surfaces.



(a) Original NASA Turbine



(b) Scaled NASA Turbine

Figure 20.—Sample three-dimensional particle trajectories ingested at 50 percent gas velocity within 5 percent of stator blade span near the hub and shroud ingested 50 percent gas velocity.

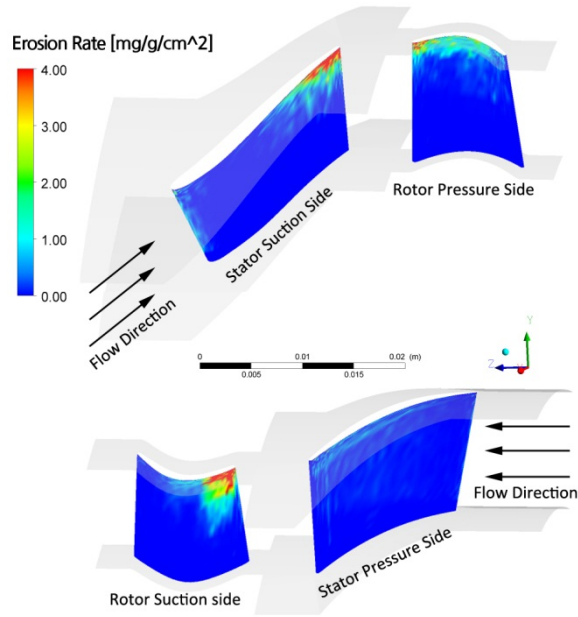


Figure 21.—TBC erosion rate predictions on blade surfaces in the NASA designed original turbine for particles ingested at 50 percent of the gas velocity for uniform radial loading.

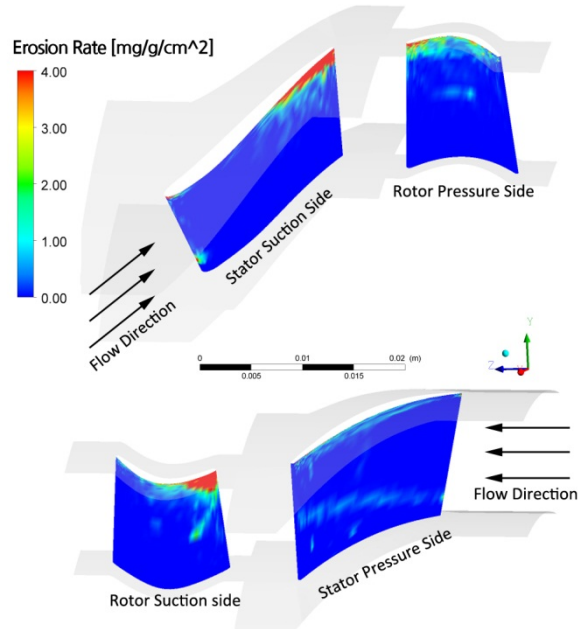


Figure 22.—TBC erosion rate prediction on blade surfaces in the NASA designed original turbine for particles ingested at 50 percent of the gas velocity within 5 percent of stator blade span near the hub and shroud.

Lower erosion rates are predicted in the case of scaled turbine. Figures 23 and 24 present the computed thermal barrier coating erosion rates on the scaled NASA turbine stator and rotor blade surfaces for uniform particle seeding (Fig. 23) and for particle seeding within 5 percent of the span near the hub and shroud (Fig. 24) compared to the NASA designed original turbine (Fig. 22).

Table 4 gives a summary of the maximum local and overall predicted TBC erosion rates in both the NASA designed original and scaled turbine. The results in Table 4 indicate that both overall and maximum local TBC erosion rates are lower in the scaled turbine than the original turbine for the same particle loading distribution. This is attributed to the fact that very few particles bounce back from the rotor suction surface to impact the stator blades in the scaled NASA turbine.

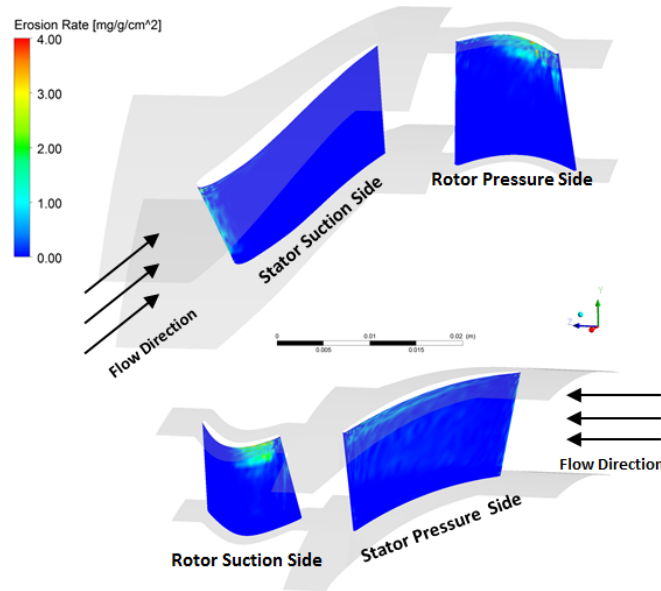


Figure 23.—TBC erosion rates on blade surfaces in the scaled NASA turbine for uniform particle loading at 50 percent of the gas velocity.

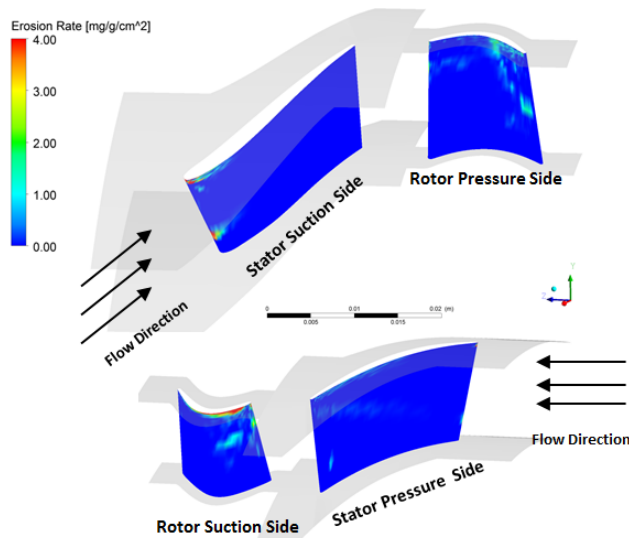


Figure 24.—TBC erosion rates on blade surfaces in the scaled NASA turbine for particles seeding within 5 percent of stator blade span near the hub and shroud at 50 percent of the gas velocity.

TABLE 4.—COMPUTED OVERALL BLADES AND MAXIMUM LOCAL TBC EROSION RATES
ON THE COMMERCIAL TURBINE AND THE NASA DESIGNED TURBINE

Turbine	Particle radial loading% span	Maximum local erosion rate, mg/g/cm ²	Overall blade erosion rate, mg/g	
			Stator	Rotor
NASA original turbine	5%	60.21 (Stator suction side)	1.50	0.88
	100%	20.43 (Stator suction side)	0.89	0.73
NASA scaled turbine	5%	21.36 (Rotor suction side)	0.28	0.43
	100%	7.66 (Rotor suction side)	0.33	0.37

After we considered all the factors that can cause such a difference, we concluded that the high flow pressures in the case of scaled NASA turbines lead to lower values of the Reynolds number for the particle slip velocities relative to the gas. Subsequently lower drag forces by the gas flow on the particles through the stator leads to lower particle velocities at the stator exit in the case of the original NASA designed turbine. Referring to Figure 14, that leads to high particle incidence angles relative to the rotor suction surface and hence lower particle rebound velocities as indicated by the experimental measured restitution blade row coefficients presented in Figure 10. Subsequently these particles do not reenter the stator blade row nor impact the stator blade surfaces.

It is interesting to compare results from the commercial APU turbine with uniform particle ingestion to those the scaled NASA designed automotive turbine with uniform particle ingestion. Both studies predict even distribution of erosion rate across the stator pressure surface with a significantly higher erosion rate on the rotor that is concentrated near the shroud. However particle trajectories in the NASA scaled turbine tended not to rebound from the rotor blade back into the stator blade row as in the original NASA and commercial APU turbine. This complex phenomenon is influenced by the several factors including the turbine blade airfoils, solidity, stator to rotor spacing as well as operating conditions.

Summary

Experimental results are presented for particle surface interactions in the form of restitution coefficients after impacts with thermal barrier coated samples over the range of impact angles and erosion rates for flow velocities and temperatures ranging between 122 m/s (400 ft/s) to 366 m/s (1200 ft/s) and 1871 °C (1600 °F) to 1093 °C (2000 °F), respectively. Predictions of TBC blade erosion by 26 μm alumina particles are presented for the different single stage axial flow turbines namely a commercial APU, NASA designed turbine and for a scaled version of the NASA designed turbine for modern rotorcraft operating conditions.

The highest overall thermal barrier coating erosion rates are always predicted on the rotor blade suction surface. On the other hand the pressure surfaces of the rotor blades always suffer the lowest thermal barrier coating erosion rates. The erosion rate of the thermal barrier coating on the stator suction surface caused by the impacts of particles that rebound from the rotor and reenter the stator blade passage is influenced by the restitution from the rotor blades suction. An important observation concerns the influence turbine flow pressure on the level of drag force on the suspended particles. This is important since the main aerodynamic force on the particles is associated with the drag coefficient that decreases with increased Reynolds number based on their slip velocity relative to gas flow.

References

1. Sirs, R.C., 1994, "The Operation of Gas Turbine Engines in Hot and Sandy Conditions-Royal Air Force Experiences in the Gulf War," AGARD-CP-558, Paper No. 2.
2. Mitchell, H.J. and Gilmore, F.R., 1982, "Dust-Cloud Effects on Aircraft Engines: Emerging Issues and New Damage Mechanisms," RDA-TR-120012-001.
3. Hamed, A., Tabakoff, W. and Wenglarz, R., 2006, "Erosion and Deposition in Turbomachinery," Journal of Propulsion and Power 22(2), pp. 350–360.

4. Mund, M.G. and Guhna, H., 1970, "Gas Turbine Dust Air Cleaners," ASME Paper 70-GT-104.
5. Mann, D.L. and Wares, G.D., 1994, "Future Direction in Helicopter Engine Protection System Configuration," AGARD-CP-588 Paper No. 4.
6. McCoy, L., 1973, "The Coal Burning Gas Turbine Project, Report of the Interdepartmental Gas Turbine Steering Committee," Australian Government Publishing Service.
7. Hamed, A., Tabakoff, W. and Wenglarz, R., 1980, "Particulate Flow and Blade Erosion," Von Karman Institute for Fluid Dynamics Lecture Series 1988-08.
8. Meier, S.M. and Gupta, D.K., 1994, "The Evolution of Thermal Barrier Coatings in Gas Turbines Engine Applications," *Journal of Engineering for Gas Turbines and Power*, 116, pp. 250-257.
9. Miller, R.A., 1989, "Life Modeling of Thermal Barrier Coatings for Aircraft Gas Turbine Engines, in: D.E. Sokolowski (Ed.), *Towards Improved Durability in Advanced Aircraft Engine Hot Sections*," NASA TM4087.
10. Meier, S.M. et al., 1991, "Thermal Barrier Coating Life Prediction Model Development," Phase II Final Report, Contract NAS3-23944, NASA CR 189111, (1991).
11. Bose, S. and Masi-Marsin, J., 1995, "Thermal Barrier Coating Experience in Gas Turbine Engines at Pratt and Whitney," *Thermal Barrier Coating Workshop*, NASA, pp. 63.
12. Tabakoff, W. and Wakeman, T., 1979, "Test Facility for Material Erosion at High Temperature," *ASTM Special Publication*, 664, pp. 123-135.
13. Tabakoff, W., 1989, "Investigation of Coating at High Temperature for Use in Turbomachinery," *Surface and Coating Technology*, 940, pp. 97-115.
14. Nicolls, J.R., Deakin, M.J. and Rickerby, D.S., 1999, "A Comparison Between the Erosion Behavior of Thermal Spray and Electron Beam Physical Vapor Deposition Thermal Barrier Coatings," *Wear*, 233-235, pp. 352-361.
15. Hussein, M.F. and Tabakoff, W., 1973, "Dynamic Behavior of Solid Particles Suspended by Polluted Air Flow in a Turbine Stage," *Journal of Aircraft* 10(7), pp. 434-440.
16. Hamed, A., Tabakoff, W., Rivir, R.B., Das K. and Arora, P., 2005, "Turbine Blade Surface Deterioration by Erosion," *Journal of Turbomachinery*, 127, pp. 445-452.
17. Hamed, A. and Tabakoff, W., 1994, "Experimental and Numerical Simulations of the Effects of Ingested Particles in Gas Turbine Engines," AGARD-CP-558, *Erosion, Corrosion and Foreign Object Effects in Gas Turbines*.
18. Roelke, R.J., and McLallin, K.L., "The Aerodynamic Design of Compressor-Drive Turbine for use in a 75 kW Automotive Engine," NASA Technical Memorandum. TMX-71717, 1975.
19. Swar, R., 2009, "Particle Erosion of Gas Turbine Thermal Barrier Coating," M.S. Thesis, School of Aerospace Systems, University of Cincinnati, Cincinnati, OH.
20. Tabakoff, W., Hamed, A. and Beacher, B., 1983, "Investigation of Gas Particle Flow in an Erosion Wind Tunnel," *Journal of WEAR*, Vol. 86, Apr, pp. 73-88.
21. Gunaraj, J.A., Tabakoff, W., and Shastri, S., 1997, "Experimental Investigation of Solid Particle Interaction in Particulate Flow," ASME Fluids Engineering Division Summer Meeting Paper No. FEDSM97-3628.
22. Gunaraj, J.A., 1997, "Study of the Effect Particle-Particle Interactions in the Particulate Flow," PhD. Thesis, University of Cincinnati.
23. Shastri, S., 1999, "Particle Rebound Characteristics of Turbomachinery Cascade Leading Edge Geometry," PhD. Thesis, University of Cincinnati.
24. ANSYS CFX, Release 12.1, User Manual, 2009.
25. Pointwise, Release 16.04, User Manual, 2011.
26. Woggon, N., "Particle Erosion of a Turbine With Restitution Analysis," M.S. Thesis, University of Cincinnati, 2012.

REPORT DOCUMENTATION PAGE			Form Approved OMB No. 0704-0188		
<p>The public reporting burden for this collection of information is estimated to average 1 hour per response, including the time for reviewing instructions, searching existing data sources, gathering and maintaining the data needed, and completing and reviewing the collection of information. Send comments regarding this burden estimate or any other aspect of this collection of information, including suggestions for reducing this burden, to Department of Defense, Washington Headquarters Services, Directorate for Information Operations and Reports (0704-0188), 1215 Jefferson Davis Highway, Suite 1204, Arlington, VA 22202-4302. Respondents should be aware that notwithstanding any other provision of law, no person shall be subject to any penalty for failing to comply with a collection of information if it does not display a currently valid OMB control number.</p> <p>PLEASE DO NOT RETURN YOUR FORM TO THE ABOVE ADDRESS.</p>					
1. REPORT DATE (DD-MM-YYYY) 01-04-2013		2. REPORT TYPE Technical Memorandum		3. DATES COVERED (From - To)	
4. TITLE AND SUBTITLE Combined Experimental and Numerical Simulations of Thermal Barrier Coated Turbine Blades Erosion			5a. CONTRACT NUMBER		
			5b. GRANT NUMBER		
			5c. PROGRAM ELEMENT NUMBER		
6. AUTHOR(S) Hamed, Awatef; Tabakoff, Widen; Swar, Rohan; Shin, Dongyun; Woggon, Nathania; Miller, Robert			5d. PROJECT NUMBER NNX07AC69A		
			5e. TASK NUMBER		
			5f. WORK UNIT NUMBER WBS 877868.02.07.03.01.03.01		
7. PERFORMING ORGANIZATION NAME(S) AND ADDRESS(ES) National Aeronautics and Space Administration John H. Glenn Research Center at Lewis Field Cleveland, Ohio 44135-3191			8. PERFORMING ORGANIZATION REPORT NUMBER E-18648		
9. SPONSORING/MONITORING AGENCY NAME(S) AND ADDRESS(ES) National Aeronautics and Space Administration Washington, DC 20546-0001			10. SPONSORING/MONITOR'S ACRONYM(S) NASA		
			11. SPONSORING/MONITORING REPORT NUMBER NASA/TM-2013-217857		
12. DISTRIBUTION/AVAILABILITY STATEMENT Unclassified-Unlimited Subject Category: 26 Available electronically at http://www.sti.nasa.gov This publication is available from the NASA Center for AeroSpace Information, 443-757-5802					
13. SUPPLEMENTARY NOTES					
14. ABSTRACT A combined experimental and computational study was conducted to investigate the erosion of thermal barrier coated (TBC) blade surfaces by alumina particles ingestion in a single stage turbine. In the experimental investigation, tests of particle surface interactions were performed in specially designed tunnels to determine the erosion rates and particle restitution characteristics under different impact conditions. The experimental results show that the erosion rates increase with increased impingement angle, impact velocity and temperature. In the computational simulations, an Euler-Lagrangian two stage approach is used in obtaining numerical solutions to the three-dimensional compressible Reynolds Averaged Navier-Stokes equations and the particles equations of motion in each blade passage reference frame. User defined functions (UDF) were developed to represent experimentally-based correlations for particle surface interaction models which were employed in the three-dimensional particle trajectory simulations to determine the particle rebound characteristics after each surface impact. The experimentally based erosion UDF model was used to predict the TBC erosion rates on the turbine blade surfaces based on the computed statistical data of the particles impact locations, velocities and angles relative to the blade surface. Computational results are presented for the predicted TBC blade erosion in a single stage commercial APU turbine, for a NASA designed automotive turbine, and for the NASA turbine scaled for modern rotorcraft operating conditions. The erosion patterns in the turbines are discussed for uniform particle ingestion and for particle ingestion concentrated in the inner and outer 5 percent of the stator blade span representing the flow cooling the combustor liner.					
15. SUBJECT TERMS Coatings; Erosion; Computational fluid dynamics					
16. SECURITY CLASSIFICATION OF:			17. LIMITATION OF ABSTRACT UU	18. NUMBER OF PAGES 28	19a. NAME OF RESPONSIBLE PERSON STI Help Desk (email: help@sti.nasa.gov)
a. REPORT U	b. ABSTRACT U	c. THIS PAGE U			19b. TELEPHONE NUMBER (include area code) 443-757-5802

